Electronic dispersion compensation using full optical-field reconstruction in 10Gbit/s OOK based systems

J. Zhao*, M. E. McCarthy, and A. D. Ellis

Photonic Systems Group, Tyndall National Institute, University College Cork, Cork, Ireland
**Corresponding author: jian.zhao@tyndall.ie*

Abstract: We investigate the design of electronic dispersion compensation (EDC) using full optical-field reconstruction in 10Gbit/s on-off keyed transmission systems limited by optical signal-to-noise ratio (OSNR). By effectively suppressing the impairment due to low-frequency component amplification in phase reconstruction, properly designing the transmission system configuration to combat fiber nonlinearity, and successfully reducing the vulnerability to thermal noise, a 4.8dB OSNR margin can be achieved for 2160km single-mode fiber transmission without any optical dispersion compensation. We also investigate the performance sensitivity of the scheme to various system parameters, and propose a novel method to greatly enhance the tolerance to differential phase misalignment of the asymmetric Mach-Zehnder interferometer. This numerical study provides important design guidelines which will enable full optical-field EDC to become a cost-effective dispersion compensation solution for future transparent optical networks.

OCIS codes: (060.2330) Fiber optics communications; (060.4080) Modulation

References and links

1. S. Schube and M. Mazzini, "Testing and interoperability of 10GBASE-LRM optical interfaces," IEEE Commun. Mag. **45**, s26-s31 (2007).
2. F. Buchali, H. Bulow, W. Baumert, R. Ballentin, and T. Wehren, "Reduction of the chromatic dispersion penalty at 10Gbit/s by integrated electronic equalizers," in *Proc. Optical Fiber Communication Conference* (2000), paper ThS1-1.
3. A. Farbert, S. Langenbach, N. Stojanovic, C. Dorschky, T. Kupfer, C. Schulien, J.-P. Elbers, H. Wernz, H. Griesser, and C. Glingener, "Performance of a 10.7 Gb/s receiver with digital equaliser using maximum likelihood sequence estimation," *European Conference on Optical Communication* (2004), PDP Th4.1.5.
4. D. McGhan, M. O'Sullivan, M. Sotoodeh, A. Savchenko, C. Bontu, M. Belanger, and K. Roberts, "Electronic dispersion compensation," in *Proc. Optical Fiber Communication Conference* (2006), paper OWK1.
5. G. Bosco and P. Poggiolini, "Long-distance effectiveness of MLSE IMDD receivers," IEEE Photo. Technol. Lett. **18**, 1037-1039 (2006).
6. M. G. Taylor, "Coherent detection for optical communications using digital signal processing," in *Proc. Optical Fiber Communication Conference* (2007), paper OMP1.
7. A. D. Ellis and M. E. McCarthy, "Receiver-side electronic dispersion compensation using passive optical field detection for low cost 10Gbit/s 600 km-reach applications," in *Proc. Optical Fiber Communication Conference* (2006), paper OTuE4.
8. X. Liu, S. Chandrasekhar, and A. Leven, "Digital self-coherent detection", Opt. Express **16**, 792-803 (2008).
9. N. Kikuchi, K. Mandai, S. Sasaki, and K. Sekine, "Proposal and first experimental demonstration of digital incoherent optical field detector for chromatic dispersion compensation," *European Conference on Optical Communication* (2006), PDP Th4.4.4.
10. A. Polley and S. E. Ralph, "Receiver-side adaptive opto-electronic chromatic dispersion compensation," in *Proc. Optical Fiber Communication Conference* (2007), paper JThA51.
11. J. Zhao, M. E. McCarthy, P. Gunning, and A. D. Ellis, "Dispersion tolerance enhancement in electronic dispersion compensation using full optical-field reconstruction," in *Proc. Optical Fiber Communication Conference* (2008), paper OWL3.
12. H. Haunstein and R. Urbansky, "Application of electronic equalization and error correction in lightwave systems," *European Conference on Optical Communication* (2004), paper Th1.5.1.

#97678 - $15.00 USD Received 19 Jun 2008; revised 25 Jul 2008; accepted 25 Jul 2008; published 15 Sep 2008

13. M. C. Jeruchim, "Techniques for estimating the bit error rate in the simulation of digital communication systems," IEEE J. Sel. Areas Commun. **SAC-2**, 153-170 (1984).
14. X. Liu and D. A. Fishman, "A fast and reliable algorithm for electronic pre-equalization of SPM and chromatic dispersion," in *Proc. Optical Fiber Communication Conference* (2006), paper OThD4.
15. B. Franz, F. Buchali, D. Rosener, and H. Bulow, "Adaptation techniques for electronic equalizers for the mitigation of time-variant distortions in 43Gbit/s optical transmission systems," in *Proc. Optical Fiber Communication Conference* (2007), paper OMG1.

1. Introduction

Electronic dispersion compensation (EDC) has attracted much interest recently due to its cost effectiveness and adaptive equalization capability for extending reach in legacy multimode optical fiber [1] as well as in metro and long-haul optical transmission systems [2-4]. The receiver-side EDC, which adapts quickly to changes in link conditions, is of particular value for future transparent optical networks where the reconfigurability of the add- and drop-nodes causes the transmission paths to vary. However, the performance of the conventional EDC using direct detection (DD EDC) is limited due to loss of the phase information. In addition, the transformation of linear optical impairments arising from chromatic dispersion (CD) into nonlinear impairments after square-law detection significantly increases the operational complexity of the DD EDC. In simulations, an optimal DD EDC using maximum likelihood sequence estimation (MLSE) was predicted to achieve 700km single mode fiber (SMF) transmission, but at the expense of increased electronic processing complexity requiring 8192 Viterbi processor states [5]. EDC based on coherent detection can access both the intensity and the phase of the optical field, allowing for full CD compensation with reduced EDC complexity [6]. However, it requires complicated optical implementations due to polarization and phase tracking between the local oscillator and the signal.

Recently, a novel cost-effective EDC receiver was proposed, which accesses the intensity and instantaneous frequency information simultaneously, using a single asymmetric Mach-Zehnder interferometer (AMZI) for on-off keyed (OOK) signals [7] or two AMZIs for differential phase shift keyed/differential quadrature phase shift keyed signals [8,9]. This recovered information allows for full optical-field CD compensation with a dispersive transmission line [7] or finite impulse response filter [8-10] in the electrical domain. In OOK based systems, this scheme was experimentally verified to successfully recover a 10Gbit/s signal after transmission over 248km of field-installed SMF [11].

While the basic concept was proposed and feasibility verified previously [7-11], a systematic investigation of the important design criteria for a practical EDC receiver using full optical-field reconstruction and limited by signal-to-noise ratio (OSNR) remained to be accomplished. In this paper, we will study the critical impairments which degrade the performance of the scheme, and accordingly propose effective solutions that enable the achievement of 4.8dB OSNR margin after 2160km SMF transmission for OOK data without optical dispersion compensation.

2. Principle and simulation model

Figure 1 depicts the principle of full optical-field EDC. The incoming optical signal is processed by a single AMZI with a differential time delay (DTD) of Δt and differential phase shift of $\pi/2$. Assuming that the input optical field (baseband representation) is $E(t)$, the two outputs of the AMZI, $E_1(t)$ and $E_2(t)$, are given by:

$$E_1(t) = (E(t) - E(t+\Delta t)e^{(j\pi/2)})/2 \approx E(t+\Delta t/2)e^{(j\pi/4)}[e^{(-j\Delta\omega(t)\Delta t/2 - j\pi/4)} - e^{(j\Delta\omega(t)\Delta t/2 + j\pi/4)}]/2$$
$$E_2(t) = (E(t) + E(t+\Delta t)e^{(j\pi/2)})/2 \approx E(t+\Delta t/2)e^{(j\pi/4)}[e^{(-j\Delta\omega(t)\Delta t/2 - j\pi/4)} + e^{(j\Delta\omega(t)\Delta t/2 + j\pi/4)}]/2 \quad (1)$$

#97678 - $15.00 USD Received 19 Jun 2008; revised 25 Jul 2008; accepted 25 Jul 2008; published 15 Sep 2008

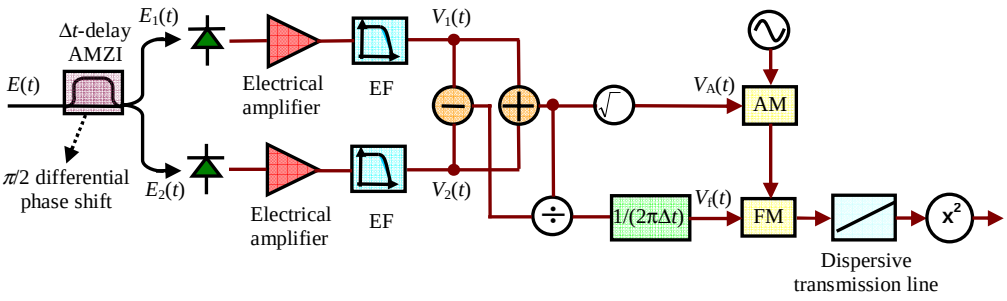

Fig. 1. Principle of full optical-field EDC

where $\Delta\omega(t)$ ($=\omega(t)-\omega_0$) is the instantaneous frequency of baseband representation of the optical field, $E(t)$. ω_0 is the optical carrier frequency. $E_1(t)$ and $E_2(t)$ are detected by a pair of detectors, electrically amplified, and filtered by electrical filters (EFs) to obtain the electrical signals $V_1(t)$ and $V_2(t)$:

$$V_1(t) = \alpha_1 \left|E(t+\Delta t/2)\right|^2 \sin^2(\Delta\omega(t)\Delta t/2+\pi/4)$$
$$V_2(t) = \alpha_2 \left|E(t+\Delta t/2)\right|^2 \cos^2(\Delta\omega(t)\Delta t/2+\pi/4) \quad (2)$$

where α_1 and α_2 are scaling factors taking account of the responsivities of the detectors and the gains of the electrical amplifiers for the $V_1(t)$ and $V_2(t)$ signal paths. For analytical simplicity, $\alpha_1=\alpha_2=1$ is assumed. Signals proportional to the intensity, instantaneous frequency, and phase information of the optical field, $V_A(t)$, $V_f(t)$, and $V_p(t)$, can be extracted by signal processing of $V_1(t)$ and $V_2(t)$:

$$V_A(t) = [V_1(t)+V_2(t)]^{1/2} = \left|E(t+\Delta t/2)\right|$$
$$V_f(t) = [V_1(t)-V_2(t)]/[2\pi\Delta t V_1(t)+2\pi\Delta t V_2(t)] = \sin(\Delta\omega(t)\Delta t)/(2\pi\Delta t) \approx \Delta\omega(t)/2\pi$$
$$V_p(t) = 2\pi\int V_f(\tau)d\tau \approx \varphi(t) \quad (3)$$

where $\sin(\Delta\omega(t)\Delta t)/(2\pi\Delta t)\approx\Delta\omega(t)/2\pi$ is satisfied given $\Delta\omega(t)\Delta t<<1$. The intensity and frequency information is exploited to reconstruct a replica of the optical signal in the radio frequency (RF) range by applying the signals V_A and V_f to amplitude and frequency modulators respectively, allowing for subsequent full optical-field compensation using a dispersive transmission line [7]. This scheme features better compensation performance compared to conventional DD EDC as it benefits from the knowledge of the recovered phase information, and also better cost effectiveness compared to the coherent-detection based EDC by avoiding complicated phase and polarization tracking or recovery.

In Fig. 1, it is shown that with proper electrical circuit design, a pair of detectors would be sufficient to access both the intensity and phase information. However, well known difficulties arise in matching the response of two independent receiver chains. Therefore, in this paper, we adopt an equivalent implementation using a balanced photodiode to give V_1-V_2 and an additional single photodiode to obtain V_1+V_2 [11].

Figure 2 shows the simulation model used in this paper, including a number of additional signal processing refinements reported in subsequent sections. Continuous wave light was intensity modulated by a 10Gbit/s OOK data train using a Mach-Zehnder modulator (MZM). The data train consisted of a 2^{11}-1 pseudo-random binary sequence (PRBS) repeated nine times (18,423 bits). 10 ‘0’ bits and 11 ‘0’ bits were added before and after this data train respectively to simplify the boundary conditions. The bits were raised-cosine shaped with a roll-off coefficient of 0.4 and 40 samples per bit. The extinction ratio (ER) of the modulated OOK signal was set by adjusting the bias and the amplitude of the electrical OOK data.

#97678 - $15.00 USD Received 19 Jun 2008; revised 25 Jul 2008; accepted 25 Jul 2008; published 15 Sep 2008

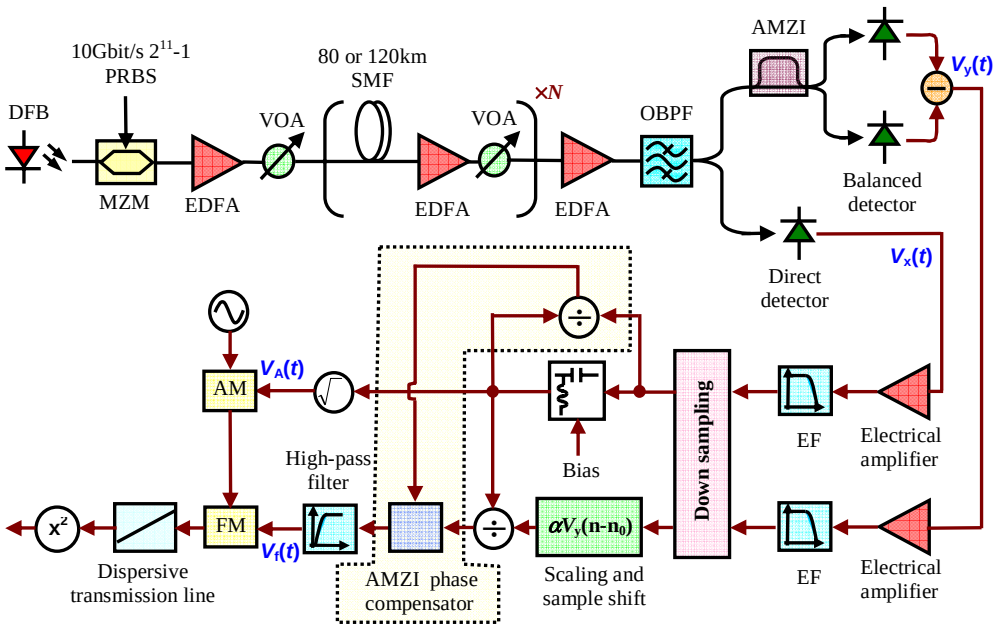

Fig. 2. Simulation model

The signal was launched into the transmission link, whose configuration including the fiber length and launch power per span has significant impact on the system performance. In this paper, two cases were investigated: (1) 80km SMF per span; (2) 120km SMF per span. The SMF was assumed to have CD of 16ps/km/nm, a nonlinear coefficient of 1.2/km/W, and a loss of 0.2dB/km. The split-step Fourier method was used to calculate the signal propagation in the fibers. At the end of each span, noise from optical amplifiers was modelled as complex additive white Gaussian noise with zero mean and a power spectral density of $n_{sp}h\nu(G\text{-}1)$ for each polarization, where G and $h\nu$ are the amplifier gain and the photon energy respectively. n_{sp} is population inversion factor of the amplifiers and was set to give 4dB amplifier noise figure (NF).

The noise of the optical preamplifier was also modelled as additive white Gaussian noise with random polarization. The launch power into the preamplifier was adjusted to control the OSNR while the output power was varied to investigate the influence of thermal noise. The pre-amplified signal was filtered by an 8.5GHz Gaussian-shaped optical band-pass filter (OBPF) which suppressed the optical noise and CD to a certain extent [12]. The signal after the OBPF was then split into two paths to extract $V_x(t)$ and $V_y(t)$, as shown in Fig. 2. The AMZI for the extraction of $V_y(t)$ had $\pi/2$ differential phase shift and DTD of either 10ps or 30ps. The responsivities of the balanced detector and the direct detector were assumed to be 0.6A/W and 0.9A/W respectively, and equivalent thermal noise spectral power densities were assumed to be 100pA/Hz$^{1/2}$ and 18pA/Hz$^{1/2}$ respectively. These receiver parameters match typical values of the commercial detectors used in the recent experimental demonstration [11]. After detection, the signals were electrically amplified, filtered by 15GHz 4th-order Bessel electrical filters (EFs), and down-sampled to 50Gsamples/s (5 samples per bit at 10Gbit/s) to simulate the sampling effect of the commonly implemented real-time oscilloscope. The down-sampled copy of $V_x(t)$ was re-biased, which can significantly enhance the robustness of the scheme to thermal noise. To allow for path length variations due to manufacturing tolerance, temperature variations and device aging, a sample shifting was included to provide delay tunability with a resolution equivalent to the sampling interval (20ps), and the amplitude was adjusted to correct for the scaling constant which equals $1/(2\pi\Delta t)$ and any gain imbalance. As will be discussed later, additional signal processing stages included a phase compensator to

#97678 - $15.00 USD Received 19 Jun 2008; revised 25 Jul 2008; accepted 25 Jul 2008; published 15 Sep 2008

significantly enhance the tolerance of differential phase misalignment of AMZI and a Gaussian-shaped high-pass EF to suppress the impairment from low-frequency amplification. $V_A(t)$ and $V_f(t)$ in Fig. 2 thus represent the recovered intensity and instantaneous frequency respectively. This information was exploited to reconstruct a replica of the optical signal, which was subsequently compensated using a dispersive transmission line. The compensated signal was then square-law detected and decoded using optimal threshold detection.

The simulation was iterated seven times with different random number seeds to give a total of 128,961 simulated bits. The performance was evaluated in terms of the required OSNR to achieve a bit error rate (BER) of 5×10^{-4} by direct error counting. 128,961 bits were sufficient to produce a confidence interval of [3.5×10^{-4} 7×10^{-4}] for this BER with 99% certainty [13].

3. Suppression of low-frequency component amplification

The performance of the full optical-field EDC greatly depends on the quality of the phase estimation, which was found to be degraded by the impairment from low-frequency amplification. To illustrate the origin of such an impairment, we may take the Fourier transform to relate the estimated phase $V_p(t)$ to the estimated frequency $V_f(t)$:

$$V_p(t) = 2\pi\int_0^t V_f(\tau)d\tau \quad \xrightarrow{F} \quad \psi_p(\omega) = 2\pi\psi_f(\omega)/(j\omega) \tag{4}$$

where $\psi_p(\omega)$ and $\psi_f(\omega)$ are the spectra of the two electrical signals $V_p(t)$ and $V_f(t)$ respectively. It is clear from Eq.(4) that the low-frequency components of $V_f(t)$ dominate phase reconstruction, with a scaling factor of $2\pi/|\omega|$. Therefore, any noise or inaccuracy in the low-frequency components of the estimated $V_f(t)$ will accumulate and eventually limit the performance of the EDC. This suggests that the low-frequency components of $V_f(t)$ should be minimized.

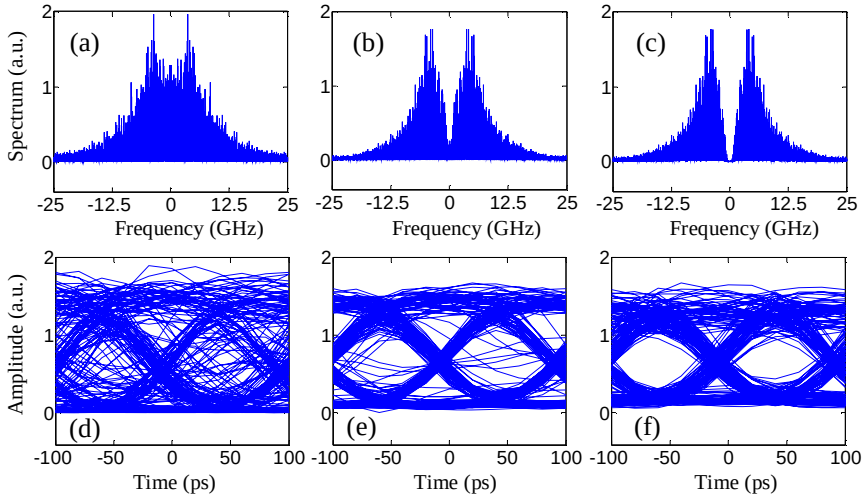

Fig. 3. Spectra of $V_f(t)$,$\psi_f(\omega)$, [(a)-(c)] and eye diagrams of the signal after dispersion compensation [(d)-(f)] at a fiber length of 2160km [(a) and (d): 25dB ER without a high-pass EF; (b) and (e): 12dB ER without a high-pass EF; (c) and (f): 12dB ER with a 0.85GHz high-pass EF].

To achieve this, we propose the employment of a reduced ER to minimize the occurrence of such low-frequency components and a high-pass EF to suppress the impairment from their amplification. To simplify the analysis in this section of the paper, fiber nonlinearity and thermal noise were not considered, but will be included in the subsequent sections. The fiber

#97678 - $15.00 USD Received 19 Jun 2008; revised 25 Jul 2008; accepted 25 Jul 2008; published 15 Sep 2008

length per span was 80km. The DTD of the AMZI and the bias of $V_x(t)$ were assumed to be 10ps and 0V respectively. Figure 3 shows $\psi_f(\omega)$ [(a)-(c)] and eye diagrams of the signal after dispersion compensation [(d)-(f)] at a fiber length of 2160km under various conditions [(a) and (d): 25dB ER without a high-pass EF; (b) and (e): 12dB ER without a high-pass EF; (c) and (f): 12dB ER with a 0.85GHz high-pass EF]. For a larger ER [(a) and (d)], the received value of $V_A(t)$ for a sequence of consecutive logical data '0's was so small that any optical noise led to large estimation inaccuracy in $V_f(t)=V_y(t)/V_A(t)^2$. This inaccuracy contained significant low-frequency content, which was further increased by the low-frequency component amplification. By using a smaller ER [(b) and (e)], the value of $V_A(t)$ for a sequence of consecutive logical data '0's was increased, reducing the estimation inaccuracy of V_f. Furthermore, the positive and negative chirps of the dispersed optical signal were detected at all points in the signal, substantially reducing the low-frequency content of V_f. Consequently, the low-frequency component amplification in the phase reconstruction was also alleviated, leading to better compensation performance at a smaller ER, as shown in Fig. 3(e). The high-pass EF in the frequency estimation path further reduced the low-frequency components of V_f. As a result, the compensated OOK signal after 2160km transmission shown in Fig. 3(f) has a significantly clearer eye than that in Figs 3(d) and 3(e).

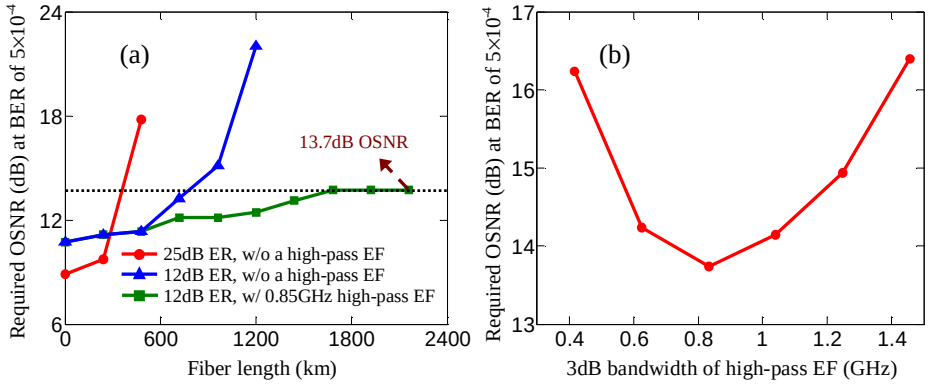

Fig. 4. (a). Required OSNR versus transmission distance (circles: 25dB ER without a high-pass EF; triangles: 12dB ER without a high-pass EF; squares: 12dB ER with a 0.85GHz high-pass EF). (b) Required OSNR versus 3dB bandwidth of the high-pass EF at a system length of 2160km and 12dB ER.

To quantify the performance improvement of the proposed methods, Fig. 4(a) depicts the required OSNR (0.1nm resolution) for the following three cases: 25dB ER without a high-pass EF (circles); 12dB ER without a high-pass EF (triangles); 12dB ER with a 0.85GHz high-pass EF (squares). The figure shows that by using 12dB ER and a 0.85GHz high-pass EF, the OSNR transmission limit could be significantly extended, despite the back-to-back penalty arising from the reduced ER. At a system length of 2160km, the required OSNR was around 13.7dB, confirming the effectiveness of the proposed method. It should be noted that whilst the high-pass EF suppresses the impairment from low-frequency component amplification, it also introduces distortion to $V_f(t)$. This distortion results in the rails of the eye diagrams in Fig. 3(f) being somewhat thicker than those in Fig. 3(e). Clearly, a trade-off exists between the impairment from low-frequency component amplification and the distortion. At an ER of 12dB, we optimized the bandwidth of the EF for 2160km transmission, which was around 0.85GHz as shown in Fig. 4(b). Note also that whilst a high-pass filter was placed in the path of V_f, no such filter was placed in the path of V_A, allowing the low-frequency components of the intensity signal $V_A(t)$ to pass through the compensator.

#97678 - $15.00 USD Received 19 Jun 2008; revised 25 Jul 2008; accepted 25 Jul 2008; published 15 Sep 2008

4. Fiber link performance

Figure 4(a) depicts the OSNR performance without fiber nonlinearity, in which case fiber link configurations do not influence the required OSNR. However, by taking the fiber nonlinearity into consideration, it would be essential to design the signal launch power and the fiber length per span to allow for sufficient OSNR margin for the transmission system. Figure 5 shows the required OSNR without (circles) and with (triangles) fiber nonlinearity and the maximum achievable OSNR (squares) for 80km SMF and -3dBm signal launch power per span. The ER was 12dB and a 0.85GHz Gaussian-shaped high-pass EF was employed. The DTD of the AMZI and the bias of $V_x(t)$ were assumed to be 10ps and 0V respectively, and photodiode thermal noise was neglected. From the figure, it is shown that including fiber nonlinearity in the transmission simulation resulted in an additional penalty of up to 1.8dB for system lengths less than 2160km. On the other hand, the maximum achievable OSNR degraded as the fiber length increased. Considering a 1550nm optical signal, 0.1nm (~12.5GHz) resolution and 4dB noise figure, for a total system length of 240km and 2160km (80km per span), the maximum achievable OSNRs were 30.2dB and 20.6dB respectively as shown by the squares in Fig. 5. In this figure, it is shown that at a fiber length of 2160km, the maximum achievable OSNR was more than 5 dB greater than the required value, confirming the significant improvement from the ER reduction and the suppression of low-frequency component amplification.

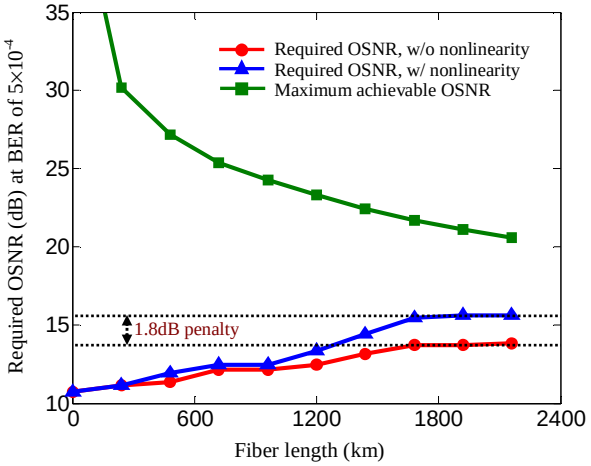

Fig. 5. Required OSNR without (circles) and with (triangles) fiber nonlinearity and the maximum achievable OSNR (squares) for 80km SMF and -3dBm signal launch power per span. The ER was 12dB and a 0.85GHz Gaussian-shaped high-pass EF was employed. The differential time delay of the AMZI and the bias of $V_x(t)$ were assumed to be 10ps and 0V respectively, and the photodiode thermal noise was neglected.

Figure 6(a) shows the required OSNR (circles) and the maximum achievable OSNR (triangles) versus signal launch power at a fiber length of 2160km with 80km per span. The other system parameters were the same as those in Fig. 5. From the figure, it is shown that for a signal launch power less than -4.5dBm, the required OSNR (circles) of 13.7 dB showed negligible penalty due to nonlinear effects. However, when the signal launch power was larger than -3dBm, the penalty induced by the fiber nonlinearity increased significantly whilst the maximum achievable OSNR increased only in proportion to the signal launch power. An optimum launch power of approximately -3dBm allowed a 5dB OSNR margin to be achieved. This trade-off between OSNR and penalty due to fiber nonlinearity is similar to that found with transmitter-side EDC [4]. Note that an additional self-phase modulation compensator [14] may be used to mitigate the nonlinear impairment, which may further enhance the OSNR margin of the systems, although this would require more complex electronic circuits.

#97678 - $15.00 USD Received 19 Jun 2008; revised 25 Jul 2008; accepted 25 Jul 2008; published 15 Sep 2008

Figure 6(b) shows the required OSNR (circles) and the maximum achievable OSNR (triangles) versus signal launch power at a fiber length of 2160km with 120km per span. It should be noted that for certain launch powers, adequate performance was not achievable. In these cases, in-line amplifier noise was neglected during simulations to allow the required OSNR to be established. From the figure, it is shown that compared to the 80km per span configuration with the same signal launch power, the required OSNR (circles) by using 120km per span was reduced for higher launch powers, due to the reduced nonlinear effect from the reduced number of spans. However, the maximum achievable OSNR decreased dramatically and as a result the OSNR margin was reduced to around 0.8dB.

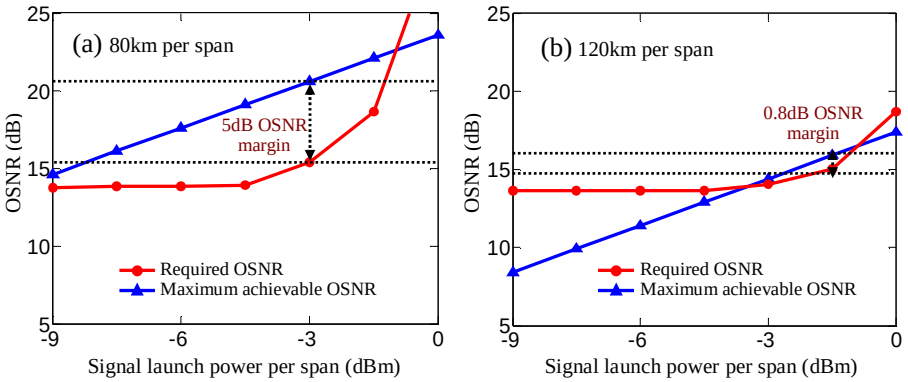

Fig. 6. Required OSNR (circles) and maximum achievable OSNR (triangles) versus signal launch power at a fiber length of 2160km with (a) 80km per span and (b) 120km per span.

5. Enhanced robustness to thermal noise

In the analysis in the following two sections, it is assumed that fiber nonlinearity is included. The system has 80km per span with a 0.85GHz Gaussian-shaped high-pass EF and the signal has the launch power of -3dBm per span and 12dB ER.

Figures 5 and 6 show the required OSNR when the thermal noise contribution of the receiver was neglected, representing the maximum achievable performance. However, in practical experimental configurations, receiver thermal noise was found to play an important role in the performance of the EDC scheme [11]. This can be attributed to the fact that the signal independent thermal noise has much more impact on the performance of phase estimation for a logical data '0' than for a logical data '1' due to the division by total received power used in the frequency estimation (Eq. (3)). This is in marked contrast to the impact of signal-spontaneous beat noise described above, where the impact of this division is mitigated by the reduced signal dependent noise for a logical data '0'.

#97678 - $15.00 USD Received 19 Jun 2008; revised 25 Jul 2008; accepted 25 Jul 2008; published 15 Sep 2008

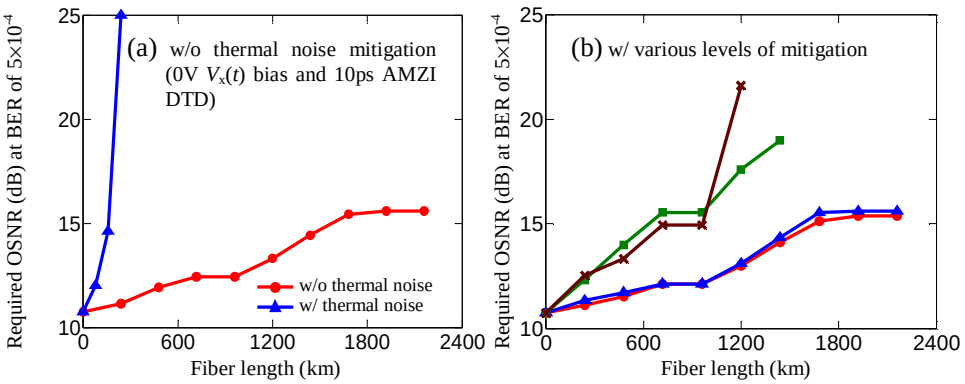

Fig. 7. (a). Required OSNR versus system length without (circles) and with (triangles) thermal noise for 0V $V_x(t)$ bias and 10ps AMZI DTD. (b) Required OSNR versus system length with various levels of thermal noise mitigation (squares: 0.1M $V_x(t)$ bias and 10ps AMZI DTD, M is defined in the text; crosses: 0V $V_x(t)$ bias and 30ps AMZI DTD; triangles: 0.1M $V_x(t)$ bias and 30ps AMZI DTD). Circles represent the case without thermal noise for 0.1M $V_x(t)$ bias and 30ps AMZI DTD. In (a) and (b), the total received optical powers of the balanced detector and direct detector were both 0dBm.

To illustrate the influence of the thermal noise, Fig. 7(a) shows the required OSNR versus the system length without (circles) and with (triangles) thermal noise for 0V $V_x(t)$ bias and 10ps AMZI DTD when the total received optical powers of the balanced detector and direct detector were both 0dBm and with the thermal noise spectral power densities as described in section 2. The figure shows that thermal noise can have significant impact on the system performance and may limit the transmission distance to less than 240km. To solve this problem, in this paper, we propose to employ an AMZI with a larger DTD (reduced free spectral range) and to bias the detected intensity signal, $V_x(t)$, to enhance the robustness of the scheme to thermal noise. Figure 7(b) shows the required OSNR versus the system length without (circles) and with (triangles) thermal noise with a 0.1M bias added to V_x and 30ps AMZI DTD (M represents the average detected signal amplitude ($[E\{| V_x(t) |^2\}]^{1/2}$) and $E\{\cdot\}$ represents the ensemble average). The system performances using either a 0.1M $V_x(t)$ bias or a 30ps AMZI DTD are also depicted in Fig. 7(b) by the squares and crosses respectively. From the figure, it is shown that without thermal noise, the proposed method had almost the same performance compared to the case of 0V $V_x(t)$ bias and 10ps AMZI DTD, as shown by the circles in Fig. 7. However, the method exhibited significantly greater tolerance to thermal noise, which we attribute to the improvement in the estimation of $V_f(t)$. Considering thermal noise alone, $V_y(t)$, $V_x(t)$, and $V_f(t)$ in Fig. 2 can be expressed as:

$$V_y(t) \propto |E(t)|^2 \Delta\omega(t)\Delta t + n_{th\_y}$$
$$V_x(t) \propto |E(t)|^2 + n_{th\_x}$$
$$V_f(t) = \frac{\alpha V_y(t)}{(V_x(t) + bias)} = \frac{|E(t)|^2 \Delta\omega(t) + n_{th\_y}/\Delta t}{2\pi(|E(t)|^2 + bias + n_{th\_x})} \quad (5)$$

where n_{th_x} and n_{th_y} represent the thermal noise on $V_x(t)$ and $V_y(t)$ respectively. The factor α accounts both for the scaling constant, which is equal to $1/(2\pi\Delta t)$, and for the potentially different gains of the $V_x(t)$ and $V_y(t)$ signal paths. $|E(t)|^2$ is very small for logical data '0's. From Eq. (5), it is clear that by employing an AMZI with a larger DTD, the output signal power from the balanced detector is increased since $V_y(t)$ is approximately proportional to Δt, which therefore improves the signal to thermal noise ratio of $V_y(t)$. Note that Δt cannot be increased infinitely because the principle for extraction of signal instantaneous frequency (Eq.

#97678 - $15.00 USD Received 19 Jun 2008; revised 25 Jul 2008; accepted 25 Jul 2008; published 15 Sep 2008

(3)) is under the assumption of small Δt ($\Delta\omega(t)\Delta t<<1$). By adding a bias on $V_x(t)$, the resultant value of the denominator for sequences of consecutive logical data '0's is increased, reducing the impact of thermal noise, although it causes slight distortions of $V_f(t)$ as well. In Fig. 8, the required OSNR versus normalized bias is plotted for 30ps AMZI DTD at a transmission length of 2160km with the total received optical powers of the balanced detector and direct detector equal to 0dBm. This figure shows that 0.1M was a near-optimum value for combating thermal noise whilst maintaining the negligible $V_f(t)$ distortion. An alternative means to combat the effect of thermal noise is to simply increase the total power incident on the photodiodes, by increasing the preamplifier gain. Figure 9 shows the required OSNR versus the total received optical power at a system length of 2160km without thermal noise mitigation, and with various levels of mitigation: (circles: 0V bias and 10ps AMZI DTD; squares: 0.1M bias and 10ps AMZI DTD; crosses: 0V bias and 30ps AMZI DTD; triangles: 0.1M bias and 30ps AMZI DTD). The dashed line represents the reference case without thermal noise described above. From the figure, it is shown that without thermal noise mitigation, a received optical power larger than 9dBm was required to achieve tolerable penalty from the thermal noise. Such strict requirement could be significantly relaxed by either properly biasing $V_x(t)$ or using a AMZI with a larger DTD. By both biasing $V_x(t)$ and using an AMZI with a larger DTD (triangles), the required optical receiver power was reduced. As a result, less than 0.3dB thermal-noise induced OSNR penalty was achieved at 0dBm received optical power. This still enables sufficient OSNR margin (~4.8dB) for the transmission system, whilst also significantly relaxing the requirements for the gain of the preamplifier, the loss of the OBPF and the AMZI, and the power handling of the detectors.

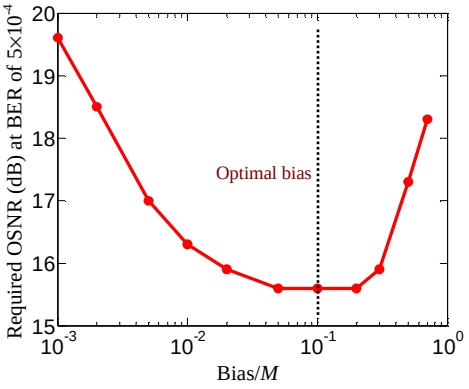

Fig. 8. Required OSNR versus normalized bias for 30ps AMZI differential time delay at a transmission length of 2160km with the total received optical powers of the balanced detector and direct detector both 0dBm.

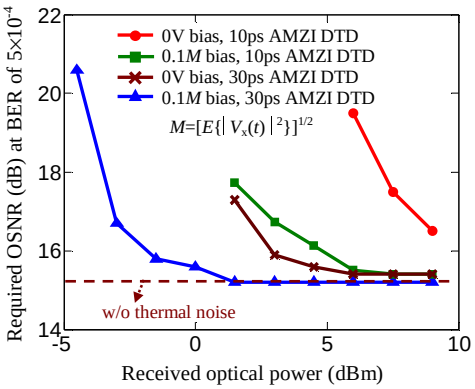

Fig. 9. Required OSNR versus total received optical power at a system length of 2160km without thermal noise mitigation and with various levels of mitigation (circles: 0V bias and 10ps AMZI DTD; squares: 0.1M bias and 10ps AMZI DTD; crosses: 0V bias and 30ps AMZI DTD; triangles: 0.1M bias and 30ps AMZI DTD).

6. Influence and compensation of variations in system parameters

The compensation system in the previous sections was assumed to be carefully optimized. For example, the differential phase of the AMZI was perfectly adjusted to be $\pi/2$ and the paths resulting in $V_x(t)$ and $V_y(t)$ were correctly matched. However, due to temperature variation and device aging, these parameters might drift over time, leading to additional OSNR penalty. Therefore, it is essential to investigate performance sensitivity to these parameters and to propose effective methods of compensation which can tolerate these kinds of drift. In

#97678 - $15.00 USD Received 19 Jun 2008; revised 25 Jul 2008; accepted 25 Jul 2008; published 15 Sep 2008

addition, it is also desirable to determine the influence of the sampling rate to understand the trade-off between performance and electronic complexity. Note that in practice, full optical-field EDC may be implemented using analogue devices, in which case some parameters, e.g. influence of sampling rate, are not relevant. In the following simulations, we assume that both fiber nonlinearity and thermal noise are included. $V_x(t)$ has a 0.1M bias and AMZI has a 30ps differential time delay.

6.1 Compensation of AMZI differential phase misalignment

Assuming that the differential phase of the AMZI is $\pi/2+\Delta\zeta$ with $\Delta\zeta$ being a misalignment, we can derive from Fig. 2:

$$V_x(t) \propto |E(t)|^2$$

$$V_f(t) = \frac{|E(t)|^2}{2\pi(|E(t)|^2 + bias)}(\Delta\omega(t) + \frac{\Delta\zeta}{\Delta t}) = \frac{|E(t)|^2}{2\pi(|E(t)|^2 + bias)}\Delta\omega(t) + \frac{|E(t)|^2}{2\pi(|E(t)|^2 + bias)}\frac{\Delta\zeta}{\Delta t} \quad (6)$$

For analytical simplicity, thermal noise on $V_x(t)$ and $V_y(t)$, which is included in Monte Carlo simulations, is not explicitly considered in Eq. (6). The first term of $V_f(t)$ in Eq. (6) estimates the instantaneous frequency ($\Delta\omega(t)/(2\pi)$) with distortions due to added bias. The second term on the right-hand side of Eq. (6) which represents the impairment from the AMZI differential phase misalignment and is linearly proportional to the misalignment $\Delta\zeta$, also introduces distortion to $V_f(t)$. The proposed AMZI differential phase compensator, included within the dotted box of Fig. 2, estimates the value of the second term and removes it from $V_f(t)$. To achieve this, $V_x(t)$ was processed to obtain $|E(t)|^2/(|E(t)|^2+bias)$ which was scaled by $\Delta\zeta/(2\pi\Delta t)$ and subtracted from the estimated frequency prior to high pass filtering. An adaptive algorithm should be used to obtain an estimation of $\Delta\zeta$ in a practical system. Adaptive feedback might be implemented for example using forward error correction (FEC) error count or an eye monitor [15]. Due to slow phase variation, it is feasible to make the convergence speed of the algorithm faster than the variation speed of the phase drift. In this paper, to simplify the analysis, we adopted static compensation for each misalignment value.

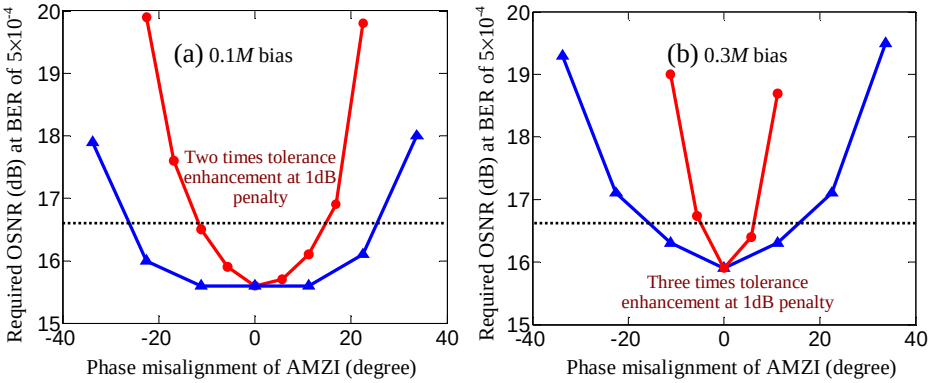

Fig. 10. Required OSNR versus differential phase misalignment at a system length of 2160km without (circles) and with (triangles) the proposed compensator for (a) 0.1M and (b) 0.3M bias.

Figure 10 shows the required OSNR versus differential phase misalignment of AMZI at a system length of 2160km without (circles) and with (triangles) the proposed compensator for (a) 0.1M bias and (b) 0.3M bias. The figure clearly shows that without the compensator, the performance of the full optical-field EDC was degraded by phase misalignment. The tolerance range at 1dB penalty was around $\pm 12^0$ in Fig. 10(a) for the optimal bias value of 0.1M. This tolerance range was reduced to $\pm 5^0$ (with respect to the reference line with optimal bias and

#97678 - $15.00 USD Received 19 Jun 2008; revised 25 Jul 2008; accepted 25 Jul 2008; published 15 Sep 2008

AMZI differential phase) by using a bias value of 0.3*M*, which introduced larger distortion and consequently more OSNR penalty when the AMZI was detuned. By using the proposed method, the sensitivity to the differential phase misalignment was greatly suppressed for both bias values. The tolerance range was significantly increased up to $\pm 24^0$ and $\pm 16^0$ at 1dB penalty for bias of 0.1*M* (Fig. 10(a)) and 0.3*M* (Fig. 10(b)) respectively, which corresponded to more than doubled tolerance compared to those without the compensator.

6.2 Sampling synchronization

Difficulties may be anticipated in matching the lengths (or delays) of the two independent receiver chains, $V_x(t)$ and $V_y(t)$, which may also change slowly with temperature and device aging. Such delay errors may be compensated using digitally implemented delays to a resolution equivalent to the sampling interval. This implies that the maximum OSNR penalty induced by poor synchronization may be estimated from the variation within this interval. Figure 11 shows the required OSNR versus delay error (D_x-(Δt/2+D_y)) at a system length of 2160km, where D_x and D_y are the delays of the path $V_x(t)$ and the path which passed through the fast arm of the Δt-delay AMZI to result in $V_y(t)$ respectively. Δt was 30ps. $V_x(t)$ was assumed to be sampled with one in five samples occurring at maximum eye opening at 50Gsamples/s. The simulated required OSNR versus delay error is clearly asymmetric, but over the optimum 20ps window, the maximum OSNR penalty is an acceptable 0.7dB.

6.3 Effect of the sampling rate

The simulations above assumed that the sampling rate was 50Gsamples/s. To quantify the impact of sampling rate, Fig. 12 shows the required OSNR versus the sampling rate at various system lengths, up to 2160km. The figure shows that the detrimental effect of reducing the sampling rate was relaxed for shorter transmission distances. For example, at a system length of 480km, the required OSNR at the minimum sampling rate of 20Gsamples/s compared to a 400Gsamples/s reference increased by 1.2dB, whilst at 2160km, the required OSNR increased by around 5dB.

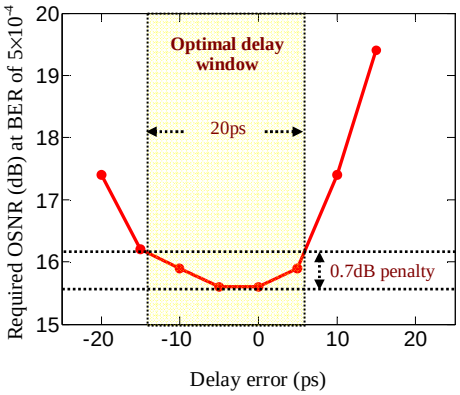

Fig. 11. Required OSNR versus delay error (D_x-(Δt/2+D_y)) at a system length of 2160km.

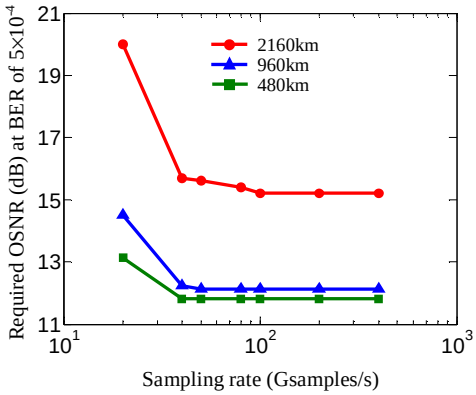

Fig. 12. Required OSNR versus sampling rate at a system length of 2160km (circles), 960km (triangles), and 480km (squares).

7. Conclusions

We have investigated the design of full optical-field EDC in 10Gbit/s OSNR limited OOK transmission systems. It was found that the most critical factors which degrade the compensation performance of the scheme are low-frequency component amplification, fiber nonlinearity, and thermal noise. We have shown that by optimizing the low-frequency response for the extracted instantaneous frequency to successfully suppress the low-frequency component amplification, phase estimation can be greatly improved. It was also shown that by

#97678 - $15.00 USD Received 19 Jun 2008; revised 25 Jul 2008; accepted 25 Jul 2008; published 15 Sep 2008

using an AMZI with a large DTD and properly biasing the detected intensity signal before optical-field reconstruction, the robustness of the scheme to thermal noise could be significantly enhanced with negligible penalty from signal distortion. By successfully suppressing these impairments and selecting an appropriate signal launch power, a 4.8dB OSNR margin may be achieved for 2160km SMF transmission using 80km span length without any optical dispersion compensation. We also investigated the performance sensitivity of the scheme to various system parameters, including the differential phase misalignment of the AMZI, unsynchronized sampling between the intensity and instantaneous frequency paths, and sampling rate. We proposed a novel compensation method to significantly enhance the tolerance of the phase misalignment of the AMZI. This numerical investigation provides important design guidelines to enable full optical-field EDC to become a cost-effective dispersion compensation solution for future transparent optical networks.

Acknowledgments

This work was supported by Science Foundation Ireland under grant number 06/IN/I969.

#97678 - $15.00 USD Received 19 Jun 2008; revised 25 Jul 2008; accepted 25 Jul 2008; published 15 Sep 2008